

FAGC: Feature Augmentation on Geodesic Curve in the Pre-Shape Space

Yuexing Han^{a,b,c,*}, Guanxin Wan^a and Bing Wang^{a,*}

^aSchool of Computer Engineering and Science, Shanghai University, 99 Shangda Road, Shanghai 200444, People's Republic of China

^bZhejiang Laboratory, Hangzhou 311100, China

^cKey Laboratory of Silicate Cultural Relics Conservation (Shanghai University), Ministry of Education

ARTICLE INFO

Keywords:

Shape space

Pre-shape space

The Geodesic curve

Feature augmentation

ABSTRACT

Deep learning has yielded remarkable outcomes in various domains. However, the challenge of requiring large-scale labeled samples still persists in deep learning. Thus, data augmentation has been introduced as a critical strategy to train deep learning models. However, data augmentation suffers from information loss and poor performance in small sample environments. To overcome these drawbacks, we propose a feature augmentation method based on shape space theory, i.e., feature augmentation on Geodesic curve, called FAGC in brevity. First, we extract features from the image with the neural network model. Then, the multiple image features are projected into a pre-shape space as features. In the pre-shape space, a Geodesic curve is built to fit the features. Finally, the many generated features on the Geodesic curve are used to train the various machine learning models. The FAGC module can be seamlessly integrated with most machine learning methods. And the proposed method is simple, effective and insensitive for the small sample datasets. Several examples demonstrate that the FAGC method can greatly improve the performance of the data preprocessing model in a small sample environment.

1. Introduction

As a powerful artificial intelligence technology, deep learning has made revolutionary breakthroughs in computer vision, natural language processing, speech recognition, and other related fields [1–3]. The training of deep learning models usually requires large amounts of labeled data to achieve excellent performance, but it is difficult to obtain large-scale and high-quality labeled data. To fully exploit the information in the small sample, data augmentation is introduced as an essential strategy to compensate for the lack of limited labeled data in training deep learning models. Data augmentation provides more learning opportunities to improve the performance and generalization of the deep learning models by expanding the training dataset and increasing the diversity of the data.

There are three main types of data augmentation methods. The first one is to use perturbation images, which add some factors to the original image, such as panning, rotating, flipping, cropping, adding noise, and other image processing methods [4]. These simple methods have some disadvantages. First, the distribution of the perturbation images ought to be close to the distribution of the original images. Furthermore, some perturbation image methods, such as translation and rotation, suffer from the padding effect. After the operation is completed, part of the image is moved out of the boundary and lost. Thus, some interpolation methods can select one of the four pixels around the blank position and fill it with the blank section [5]. These processing methods can weaken the model's attention to the critical regions and affect the model's performance. The current study tends more toward sophisticated methods, such

as Random Erasure, Mixup [6], Cutout [7], RandAugment [8], etc. These methods can improve the learning ability and generalization ability of the models of deep learning. Another type of data augmentation is generative models, which generate the virtual data from the real data, such as GANs [9] and VAEs [10]. These models have been widely used to their excellent generative capabilities. However, the generative models still rely on large data sizes, leading to the generally poor quality of images generated by these generative models in the face of limited datasets.

The third type of data augmentation method is to augment the features extracted from the data, i.e., feature augmentation. The key idea is to reshape the decision boundaries of rare categories by directly manipulating the data in the feature space and enhancing the representational ability of the data. For example, DeVries and Taylor proposed a data augmentation approach based on feature space [11]. Because they found that when traversing along a manifold, the probability of encountering real samples in the feature space is higher than in the input space. The SMOTE method selects a synthetic sample point by randomly choosing a point on the line that intersects k similar samples in feature space [12]. The DBSMOTE algorithm [13], as a derivative of SMOTE, generates new synthetic samples by calculating the distances from the cluster centers. Although the generated samples are very close to the original sample distributions, it also increases the risk of overfitting. Recently, Vikas Verma et al. proposed a new method, called manifold mixup, for training neural networks on interpolation of hidden representations [14]. The method encourages the neural network to perform uncertainty analysis of the feature space, which was not visible during the training phase and, in turn, generates more discriminative features. ISDA enhances the data samples by

*Corresponding author.

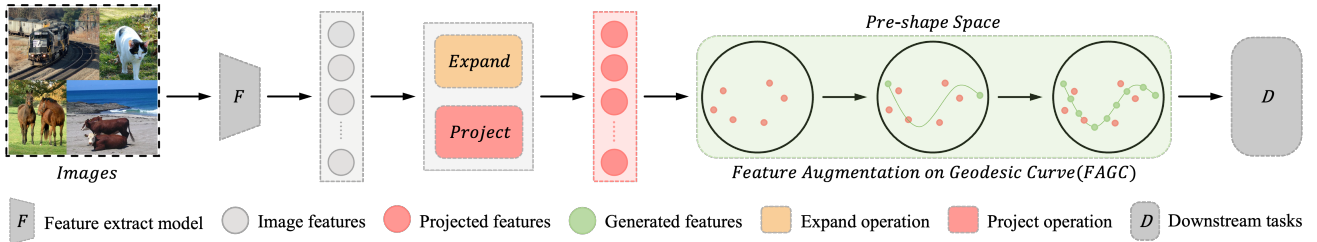


Figure 1: An overview of FAGC. The image data sequentially passes through the feature extraction module, the expand module, and the project module, which converts the image data into features and projects them into the pre-shape space. In the pre-shape space, the Geodesic curves are constructed by minimizing the sum of squares of Geodesic distance. The Geodesic curves corresponding to each category are constructed. Then, new features are generated according to the categories and given to the machine learning models to achieve the effect of feature augmentation.

transforming the CNN features along the semantic directions [15]. However, these methods always result in decreased performance and increased complexity when utilized with limited datasets.

In order to solve the shortcomings of the feature augmentation methods, this paper proposes FAGC, a feature augmentation method on Geodesic curve based on the shape space theory. The shape space theory [16–18], as a kind of manifold theory, mainly focuses on the geometric attributes, structure, and arrangement of the data. The theory has been widely used in image processing due to its remarkable interpretability of data and insensitivity to limited datasets [19–22]. For example, Kilian et al. proposed to use shape space for sampling and projection on a highly sparse collection of three-dimensional models to generate geometrically and semantically valid samples [23]. Han et al., on the other hand, proposed an object recognition method using the shape space theory. They projected object contours into shape space and constructed Geodesic curves consistent with the diverse potential shapes of a given object type [24]. In this paper, we extract features from images by a deep learning model and then project these image features into a pre-shape space. Then, the Geodesic curve fits these features and generates new features for machine learning or deep learning training. Thus, FAGC achieves data augmentation in a small sample scenario.

A concise overview of our framework is presented in Figure 1, highlighting our primary contributions as follows:

- The FAGC module can generate the data flexibly and conveniently in the small sample environments.
- A Geodesic curve is constructed to fit the projected images into pre-shape space.
- The random probability and the influence factors are introduced in the classifier module for downstream tasks.
- Empirical results demonstrate that FAGC significantly improves the performance of downstream tasks on different benchmark datasets.

2. Related Work

2.1. Pixel-level augmentation

Data augmentation has an important role in the evolution of machine learning. The earliest demonstrations of the effectiveness of data augmentation came from simple transformations such as horizontal flipping of pixels, color augmentation, and random cropping. Most of these techniques operate directly on the image and are easy to implement. Then, image augmentation methods based on image erasure, in which the main idea is to remove one or more sub-regions of an image and replace the pixel values of these sub-regions with constant or random values, were proposed. DeVries et al. proposed a simple regularisation technique called Cutout, whereby a square region of the input is randomly masked during the training of a convolutional neural network [7]. The technique improves the robustness and overall performance of the convolutional network. Singh et al. proposed Hide-and-Seek to randomly hide blocks in the training image, which forces the network to look for other relevant content while the most discriminative content is hidden [25]. Zhong et al. proposed random erasure, where a randomly selected rectangular region in the image replaces other pixels with random values [26]. In addition, some image-mixing methods mainly achieve augmentation by mixing two or more images or sub-regions of an image into a new image. Zhang et al. proposed a general synthesis method, Mixup [6]. Instead of averaging the intensities of two images, Mixup performs a convex combination of sample pairs and their labels. As a result, Mixup establishes a linear relationship between data augmentation and supervised labels and can regularize neural networks. Drawing on the idea of Mixup, Yun et al. proposed CutMix [27], which replaces the removed region with another image or images instead of simply removing pixels from the training set or mixing the images to produce a more natural image than Mixup. One obvious drawback of the augmentation technique, however, is that the mixed image itself does not make any sense from a human perspective. The performance gains from mixed images are also difficult to understand and explain. One possible explanation is that the size of the dataset enhances the ability to characterize low-level features (e.g., lines and edges).

2.2. Feature-level augmentation

Feature augmentation is mainly a method of transforming and enhancing data in feature space. In the face of image data, the traditional methods mainly focus on image extraction by feature operators to obtain more valuable feature representations to feed machine learning models. For example, SIFT [28], HOG [29], and LBP [30] feature operators can extract useful feature information from images. However, it has many drawbacks, such as the need to manually design the feature extractor and poor performance in complex scenes. With the development of deep learning, convolutional neural networks can automatically learn image feature representations without manually designing feature extractors and show more powerful generalization ability and performance. Therefore, more and more image processing methods are inclined to use convolutional neural networks for feature extraction. As an example, the stochastic feature-enhanced SFA algorithm utilizes class-conditional covariance matrix information during neural network training to improve model performance [31]. In addition, Li et al. introduced a method of implicit feature enhancement known as moment exchange [32]. The method encourages the model to use the moment information of potential features at another moment to replace the current moment information, in order to achieve the effect of feature enhancement. VAE is also suitable for feature augmentation because the decoder can reconstruct the low-dimensional representations extracted by the encoder into the original image [10]. Similarly, it is possible to augment the feature representation in a convolutional neural network in feature space by changing the output layer of the network so that the output is a low-dimensional feature instead of a category label. These features representations can train machine learning models such as plain Bayes, support vector machines, and fully connected layer networks [33], thereby improving model performance for downstream tasks. In our proposed feature augmentation method, the feature extraction process also draws on the idea, using convolutional neural networks for feature extraction, and then a series of augmentation processes are performed on the extracted features.

2.3. The shape space theory

The theory of shape space, firstly introduced by Kendall, is used to describe an object and all its equivalent variations in a non-Euclidean space [16]. In shape space, the position, scale, and orientation of a shape can be neglected. The shape space theory is often used in object recognition scenarios, where the distance between objects in shape space determines the outcome of object recognition. The feature representing the shapes of the objects are first projected into the pre-shape space, i.e., all the shapes of the features of the p coordinate points are embedded in a unit hyper-sphere [17, 34, 35], denoted as S_*^{2p-3} . Any shape is a point or vector on this hyper-sphere, and all changes in the shape, i.e., position, scale scaling, and 2D rotation, result in a new shape that lies on a great circle in S_*^{2p-3} , denoted $O(v)$, where v denotes that the shape is on S_*^{2p-3} . The set of all shapes in

the unit hyper-sphere S_*^{2p-3} forms the orbit space Σ_2^p , which is a shape space described as follows:

$$\Sigma_2^p = \{O(v) : v \in S_*^{2p-3}\}, \quad (1)$$

An example of pre-shape space and shape space is shown in Figure 2, where pre-shapes of the same polygon at different locations, scales, and orientations are all on the same great circle of S_*^{2p-3} , where the great circle serves as a point or vector in the shape space. Rather than the Euclidean distance, the Geodesic distance is the shortest distance between two points in the pre-shape space S_*^{2p-3} . Assuming that v_1 and v_2 are two features in the pre-shape space, the Geodesic distance between v_1 and v_2 is defined as [36]:

$$d(v_1, v_2) = \cos^{-1}(\langle v_1, v_2 \rangle), \quad (2)$$

where $\langle v_1, v_2 \rangle$ denotes the inner product between v_1 and v_2 . The distance between two shapes in the shape space Σ_2^p can be defined as follows [37, 38]:

$$d_p[O(v_1), O(v_2)] = \inf[\cos^{-1}(\langle \alpha, \beta \rangle) : \alpha \in O(v_1), \beta \in O(v_2)], \quad (3)$$

However, the d_p calculation in the formula is very complicated and is usually projected into the complex domain space so that Formula (3) can be described by the Procrustean distance [39]:

$$d_p[O(v_1), O(v_2)] = \cos^{-1} \left(\left| \sum_{j=1}^p v_{1j} v_{2j}^* \right| \right), \quad (4)$$

where v_{1j} and v_{2j} denote the j -th complex coordinates of v_1 and v_2 , respectively, and v_{2j}^* is denoted as the complex conjugate of v_{2j} . Subsequently, researchers found that data redundancy could be reduced based on the shape space theory for fast object recognition [40]. Further work includes calculating the Geodesic distance between two images using the corresponding feature points, thus calculating the degree of similarity of key objects in the two images [41].

In pre-shape space, points on a Geodesic curve can be used to describe a set of changing shapes. Evans et al. proposed a method to fit the data in the pre-shape space by obtaining a set of orthogonal points in the pre-shape space to construct the Geodesic curve [42, 43]. Based on this, Han et al. proposed a method to construct Geodesic curves and thus expand the data in the pre-shape space using some small amount of data, where the two endpoints of the curves can be non-orthogonal [24]. Assuming that v_1 and v_2 denote two points in the pre-shape space, the Geodesic curve formula can be derived as follows:

$$\Gamma_{(v_1, v_2)}(s) = (\cos s) \cdot v_1 + (\sin s) \frac{v_2 - v_1 \cdot \cos \theta_{(v_1, v_2)}}{\sin \theta_{(v_1, v_2)}}, \quad (0 \leq s \leq \theta_{(v_1, v_2)}) \quad (5)$$

where $\theta_{(v_1, v_2)}$ denotes the Geodesic distance between v_1 and v_2 , and s is the angle that denotes the Geodesic distance

between the new point v and v_1 . If $0 \leq s \leq \theta_{(v_1, v_2)}$, then $v_1 \leq \Gamma_{(v_1, v_2)} \leq v_2$. Following the path, a series of new data or points can be generated in the pre-shape space, and all of these points are equivalent variations between v_1 and v_2 , which is extremely helpful for expanding the size of the dataset. Based on Formula (5), the work constructs a Geodesic curve in the pre-shape space to fit the features of multiple images and generates new features along the curve to achieve feature augmentation.

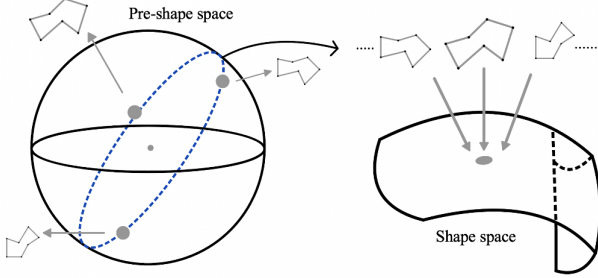


Figure 2: A pre-shape space and a shape space. A shape with different positions, scales, and orientations all lie on an orbit in the pre-shape space, while this orbit is a point in the shape space.

3. Methods

The FAGC method consists of four steps: image feature extraction, projection of the image features into the pre-shape space as features, construction of a Geodesic curve to fit the features and generation of new data along the Geodesic curve. The main steps outlined above are depicted in Figure 3.

3.1. Image feature extraction

The initial step of the FAGC method involves mapping the input data from the pixel space to the pre-shape space. Typically, the quality of features is significantly influenced by the feature extraction method. Here, we adopt the deep learning method. Complex neural network models have a tendency to extract highly discriminative features, and the utilization of high-quality features can significantly improve the performance of downstream tasks. The image features can be extracted from each layer of the neural network models. The higher layers of the network often exhibit a stronger capability to learn more intricate and comprehensive feature representations. In this paper, we employ a Vision Transformer (ViT) network [44] of which the final fully connected layer is removed as the feature extractor. The samples are fed into the pre-trained ViT network for fine-tuning, and the fine-tuning process is continued until the cross-entropy loss stabilizes. The output features from the trained ViT network represent the features in the feature space.

3.2. Projection of the image features into the pre-shape space

According to the theory of shape space, the vertices of a shape structure are typically required to be two-dimensional

or three-dimensional. Therefore, the features obtained from the ViT network need to be up-dimensioned to twice their original number before being projected into a pre-shape space and a shape space. The up-dimensioned step can be achieved by adding additional dimensions or using techniques such as interpolation or transformation to match the required dimensional space of the shape structure.

In this paper, the up-dimensioned method is to copy a feature into two identical features. The image feature is assumed to be represented as $V_0 = \{x_1, x_2, \dots, x_n\}$, where n is the dimension of the feature. Thus, the up-dimensioned function $f(x) = x$, i.e., V_0 is transformed to $V_1 = \{x_1, y_1, x_2, y_2, \dots, x_n, y_n | y_i = x_i, i \in [1, n]\}$. To mitigate the effect of the feature positions, the means of the features are removed, and the new feature $V_2 = \{x'_1, y'_1, x'_2, y'_2, \dots, x'_n, y'_n | x'_i = x_i - X_\mu, y'_i = y_i - Y_\mu, i \in [1, n]\}$, where X_μ, Y_μ are the means of $\{x_i\}$ and $\{y_i\}$, respectively. Then, the scaling of the feature V_2 is excluded with formula $z = \frac{V_2}{\|V_2\|}$, where $\|V_2\|$ means the Euclidean norm of V_2 . Thus, the image feature $\frac{V_2}{\|V_2\|}$ is projected into a pre-shape space as z .

3.3. Construction of a Geodesic curve to fit the features

To construct a Geodesic curve in the pre-shape space, more than two image samples are required. Different Geodesic curves represent different categories or classes of images. As mentioned in the above subsections, the features are extracted from the multiple images with the ViT network model, and projected into a pre-shape space, denoted as $Z = \{z_1^1, \dots, z_1^{M_1}, \dots, z_N^1, \dots, z_N^{M_N}\}$, where N represents the total number of image categories, M_i represents the number of images in the i -th category, and z_i^j denotes j -th sample of the i -th category.

The set of the Geodesic curves representing multiple image categories in the pre-shape space is denoted as $\{\Gamma_{(v_i^*, w_i^*)} | i \in (1, N)\}$, where v_i^* and w_i^* represents the optimal parameters of the Geodesic curve, as v_1 and v_2 in Formula (5). To obtain the optimal v_i^*, w_i^* of the Geodesic curve $\Gamma_{(v_i^*, w_i^*)}$, the first step is to calculate the Geodesic distance among all features. Then, the feature with the maximum sum of distances from other features is selected as the initialization parameter v_i^* , defined as follows:

$$v_i^* = \operatorname{argmax}_{z_i^k} \sum_{j=1}^{M_i} d(z_i^k, z_i^j), k \in \{1, \dots, M_i\} \quad (6)$$

where $d(z_i^k, z_i^j)$ means the Geodesic distance between z_i^k and z_i^j , calculated with Formula (2). Subsequently, w_i^* is obtained through Geodesic curve $\Gamma_{(w_i^0, w_i^1)}(\cdot)$, which is determined by the two features w_i^0 and w_i^1 furthest from v_i^* . As shown in Figure 3 (c), the two features, w_i^0 and w_i^1 , corresponding to the maximum two Geodesic distance from v_i^* , are calculated using the following formulas:

$$w_i^0 = \operatorname{argmax}_{\mathcal{Q}_i - \{v_i^*\}} (d(v_i^*, \mathcal{Q}_i - \{v_i^*\})), \text{ and} \quad (7)$$

$$w_i^1 = \operatorname{argmax}_{\mathcal{Q}_i - \{v_i^*, w_i^0\}} (d(v_i^*, \mathcal{Q}_i - \{v_i^*, w_i^0\})), \quad (8)$$

where $\mathcal{Q}_i = \{z_i^1, z_i^2, \dots, z_i^{M_i}\}$ to represent the set of features for the i -th category $\{z_i^1, z_i^2, \dots, z_i^{M_i}\}$. $\mathcal{Q}_i - \{\#\}$ means if the features $\#$ are in \mathcal{Q}_i , they are removed from \mathcal{Q}_i .

Then, a Geodesic curve $\Gamma_{(w_i^0, w_i^1)}(\cdot)$ between w_i^0 and w_i^1 is calculated with Formula (5). A set of features $\hat{w}_i^{\{1, \dots, S\}}$ is obtained by following the curve $\Gamma_{(w_i^0, w_i^1)}(\cdot)$, denoted as $\{\Gamma_{(w_i^0, w_i^1)}(s_i^1), \Gamma_{(w_i^0, w_i^1)}(s_i^2), \dots, \Gamma_{(w_i^0, w_i^1)}(s_i^S)\}$, where S represents the number of temporary features on $\Gamma_{(w_i^0, w_i^1)}(\cdot)$. Finally, among v_i^* and $\hat{w}_i^{\{1, \dots, S\}}$, several Geodesic curves $\Gamma_{(v_i^*, \hat{w}_i^{\{1, \dots, S\}})}(\cdot)$ are described. The sum of squared Geodesic distance is calculated from the i -th category of features $z_i^1, z_i^2, \dots, z_i^{M_i}$ to $\Gamma_{(v_i^*, \hat{w}_i^{\{1, \dots, S\}})}(\cdot)$. The features \hat{w}_i^* corresponding to the shortest sum is calculated as follows:

$$\hat{w}_i^* = \operatorname{argmin}_{\hat{w}_i^k} \sum_{j=1}^{M_i} \left(d(z_i^j, \Gamma_{(v_i^*, \hat{w}_i^k)}(\cdot)) \right)^2, k \in \{1, \dots, S\} \quad (9)$$

and the step is illustrated in Figure 3 (f) and Figure 3 (g). Subsequently, assign the variable w_i^* to v_i^* and calculate the two furthest features from v_i^* , as illustrated in Figure 3 (h). Repeat the steps for obtaining w_i^* as previously described in Figures 3 (i) to (j) until w_i^* and v_i^* cease to change. Consequently, $\Gamma_{(v_i^*, w_i^*)}(\cdot)$ denotes the optimal Geodesic curve fitting the distribution of feature z_i^* , as depicted in Figure 3 (k). The detailed procedure for FAGC of features for a specific category is outlined in Algorithm 1.

All Geodesic curves for different categories, denoted as $\{\Gamma_{(v_i^*, w_i^*)}(\cdot) | i \in \{1, N\}\}$, can be constructed with the above mentioned method. And, with utilizing Formula (2), the Geodesic distance $d(v_i^*, w_i^*)$ between all pairs of v_i^* and w_i^* is calculated. The distance indicates the range of the angle value s within the Geodesic curve function $\Gamma_{(v_i^*, w_i^*)}(\cdot)$. A uniform distribution $s \sim U(0, d(v_i^*, w_i^*))$ is employed to sample a set of angle values $\{s_i^j | j \in \{1, K\}\}$, where K represents the number of sampled angle values for the Geodesic curves of the i -th category. The new features $Z' = \{z_1^{\prime 1}, \dots, z_1^{\prime K}, \dots, z_N^{\prime 1}, \dots, z_N^{\prime K}\}$ are generated by substituting s_i^j into the Geodesic curve of the category i . These features and the original features from the sample image, constitute a set of expanded features $\{z_i^j, z_i^{\prime k} | i \in (1, N), j \in (1, M_i), k \in (1, K)\}$. Most machine learning models can be enhanced with the expanded features.

3.4. Design of the loss function

A good loss function can improve the performance of the machine learning model. Generally, the cross entropy loss function is chosen since it can more sensitively reflect

the differences between the predicted and true categories. In general, the number of generated features with the FAGC module is far more than the number of the original features. To balance the influence of the quantitative differences, a new loss function is proposed based on the cross entropy loss. we employ the standard cross entropy loss function, denoted as L_r , to evaluate the model's performance on original features. For the generated features, two key control factors are introduced, i.e., the random probability factor P_g and the influence factor λ . In each training batch, the final classifier loss function L_{cls} is defined as follows:

$$L_{cls} = L_r + P_g \times \lambda \times L_g. \quad (10)$$

If $P_g > 0.5$, the model is trained with the batch of the generated features. Otherwise, $P_g \leq 0$ and the generated features are ignored. P_g can be used to randomly choose partially generated features for the training process. λ can adjust the contribution of the generated features in the overall loss function. Thus, an influence balance between the original features and the generated features is controlled with P_g and λ .

Algorithm 1 Feature Augmentation on Geodesic Curve(FAGC)

Input: Features $\mathcal{Q}_i = \{z_i^1, \dots, z_i^{M_i}\}$, number of samples in i -th category M_i , number of generating features K , and number of temporary features on the Geodesic curve S .

Output: Geodesic curves $\Gamma_{(v_i^*, w_i^*)}(\cdot)$ and the generated features $Z' = \{z_i^{\prime 1}, \dots, z_i^{\prime K}\}$.

- 1: $v_i^* = \operatorname{argmax}_{z_i^k} \sum_{j=1}^{M_i} d(z_i^k, z_i^j), k \in \{1, \dots, M_i\}$;

- 2: **while** v^*, w^* not converge **do**

- 3: $w^0 = \operatorname{argmax}_{\mathcal{Q}_i - \{v_i^*\}} (d(v_i^*, \mathcal{Q}_i - \{v_i^*\}))$;

- 4: $\hat{w}_i^{\{1, \dots, S\}} = \{\Gamma_{(w^0, w^1)}(s \cdot 1), \Gamma_{(w^0, w^1)}(s \cdot 2), \dots, \Gamma_{(w^0, w^1)}(s \cdot S)\}$;

- 5: $w_i^* = \operatorname{argmin}_{\hat{w}_i^k} \sum_{j=1}^{M_i} (d(z_i^j, \Gamma_{(v_i^*, \hat{w}_i^k)}(\cdot)))^2, k \in \{1, \dots, S\}$;

- 6: Assign w_i^* to v_i^* ;

- 7: **end while**

- 8: Calculate $d(v_i^*, w_i^*)$ with Formula(2);

- 9: **for** $k = 1$ to K **do**

- 10: Sample $\hat{s}_i^k \sim U(0, d(v_i^*, w_i^*))$;

- 11: $\hat{z}_i^k = \cos(\hat{s}_i^k) \cdot v_i^* + \sin(\hat{s}_i^k) \frac{w_i^* - v_i^* \cdot \cos \theta_{(v_i^*, w_i^*)}}{\sin \theta_{(v_i^*, w_i^*)}}$;

- 12: **end for**

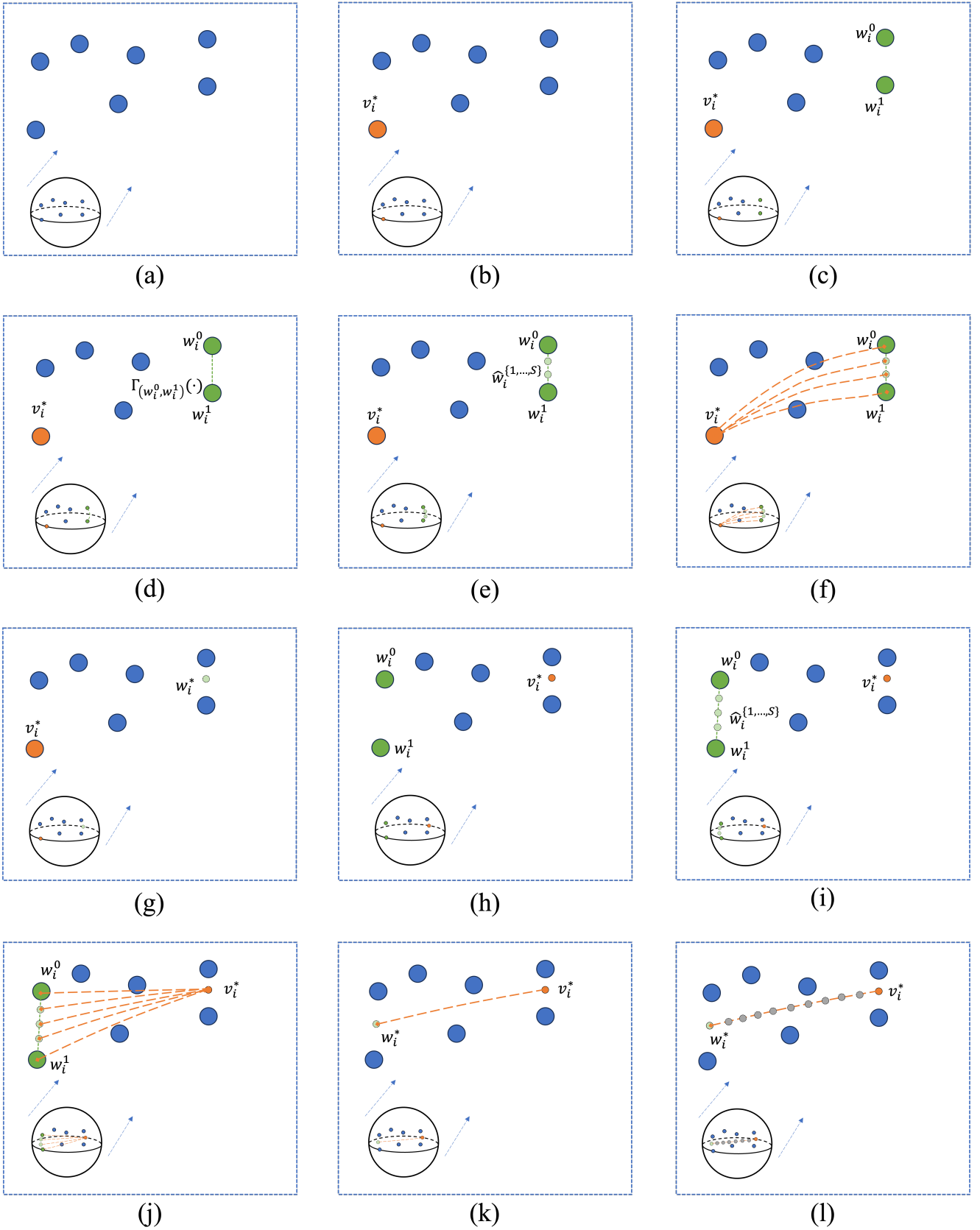


Figure 3: The process of the FAGC method. The hyper-sphere is a pre-shape space; the blue solid dots indicate the features in the pre-shape space; the solid orange dots represent features for parameter v_i^* ; the solid green dots represent the two farthest known features w_i^0 and w_i^1 from features v_i^* ; (a) Projection of image features to the pre-shape space; (b) Initialization of parameter v_i^* . From (c) to (g), the process of finding w_i^* ; From (h) to (k), the process of finding new v_i^* ; (l) Obtaining an optimal Geodesic curve $\Gamma_{(v_i^*, w_i^*)}(\cdot)$.

4. Experiments

Two datasets are utilized in the subsequent experiments. First, the proposed FAGC module is combined with various advanced learning methods and the process results demonstrate the FAGC module’s effectiveness. Then, the proposed method is compared with some data augmentation methods. Finally, some ablation experiments about classifiers are executed to check the influence of the number of features generated by FAGC. The two datasets are CIFAR-10 [45] and CIFAR-100 [45]. The benchmark methods include CoMatch [46], Π -Model [47], Mean Teacher [48], Pseudo Labeling [49], MixMatch [50], VAT [51], Dash [52], CRMATCH [53], UDA [54], FixMatch [55], FlexMatch [56], FreeMatch [57], AdaMatch [58], SimMatch [59], SoftMatch [60].

4.1. Efficiently performing FAGC

The FAGC module is combined with various state-of-the-art learning methods on the CIFAR-10 and CIFAR-100 datasets [45]. CIFAR-10 and CIFAR-100 are benchmark datasets comprising 50,000 training and 10,000 test images, which are in color and have a resolution of 32×32 pixels. CIFAR-100 shares the identical image set with CIFAR-10, consisting of 100 categories, with each category comprising 600 images. The training set is partitioned into labeled and unlabeled subsets, respectively. The numbers of samples per category for two experiments on the CIFAR-10 are 4 and 20, respectively. Thus, the total labeled samples are 40 and 200 for the two experiments, respectively. Similarly, for the CIFAR-100 dataset, we maintain the same sample ratios, yielding labeled samples of 400 and 2000 for the two scenarios.

We employ the ViT [44] network as the feature extraction model for CIFAR-10 and CIFAR-100 datasets, which are preprocessed with the methods of horizontal flips and random crops. Considering the image size of the CIFAR-100 dataset, the input scale of the standard ViT is adjusted to accommodate 32×32 image input and patch size of 2. The dimensions of the intermediate hidden layer, its depth, and the number of projection heads are set to 384, 12, and 6, respectively. The adjusted ViT is referred to as ViT-S [44]. Similarly, given the smaller number of categories in the CIFAR-10 dataset, we adopt the lightweight ViT-T [44] as the backbone network. It differs from the ViT-S structure in which the dimensions of the intermediate hidden layer are 192, and the number of projection heads is 3. We utilize the standard cross-entropy loss and utilize AdamW [61] as the optimizer. Additional configurations include a learning rate weight decay 0.0005, a learning rate 0.0005, a layer decay rate 0.5, and a moving average momentum 0.9.

In our comparative analysis, the FAGC module is integrated with different learning models of which source codes are referenced from USB [62]. For each model, we gather experimental results from the last 10 epochs which are used to calculate the average accuracy. Simultaneously, we report a 95% confidence interval. The results are shown in Table 1. Obviously, FAGC combines different models to enhance the performance of the original model. Particularly, for the 400

labeled images in CIFAR-100, FAGC achieves an average classification accuracy improvement of approximately 4%. For the labeled images in CIFAR-10, FAGC exhibits a significant improvement when utilizing 40 labeled images. However, the enhancement of FAGC is not significant if the number of training samples is large, such as 200 labeled images in CIFAR-10. This is because the backbone network is more thoroughly trained with 400 images, and its accuracy reaches 90.13%.

To describe the influence of the FAGC module combined with the neural networks, the FAGC module is combined with ViT-T, ViT-S, WRN-28-2 [63], and WRN-28-8 [63] in supervised training. As shown in Table 2, the performance of the models are significantly improved by the FAGC module. With the increase of the training samples, the influence of the FAGC module is decreased. Therefore, the FAGC module is more suitable for the small samples.

4.2. The effectiveness of FAGC in data augmentation methods

To evaluate the effectiveness of the FAGC module, we choose several representative augmentation methods which include horizontal flip, rotate, random crop, color jitter, cutout and augmix [64]. An experiment is executed by ViT-S with some data augmentation methods and FAGC for 400 labeled images in CIFAR-10. Table 3 describes the comparison of these methods whether to combine or not combine the FAGC module. From Table 3, the FAGC module can improve the classification accuracy combined with other data augmentation methods. It is noteworthy that the combination of all data augmentation methods does not achieve optimal classification accuracy, as shown in ID 8. In contrast, optimal accuracy is achieved with the combination of the methods of horizontal flip, random crop and the FAGC module.

4.3. The influence of machine learning models on FAGC

Two experiments that choose 40 and 200 images from CIFAR-10 as training sets, respectively, are executed to understand the influence of the FAGC module on the feature classifiers. The feature extraction network model is ViT-S, and the feature classifiers for comparison include KNN [65], SVC [66], DecisionTree [67], ExtraTree [68], RandomForest [69], Bagging [70], GradientBoost [71] and MLP [72]. The results indicate that the FAGC module can improve the performance of the machine learning models, as shown in Table 4. Moreover, the MLP with the FAGC module as the highest classification accuracy. Since MLP uses the output layer weight parameters of the ViT-S.

4.4. The influence of the number of generated features on the model

To evaluate the influence of the number of generated features for the models, we use multiple machine learning models as classifiers trained on 400 labeled features in CIFAR-100, including KNN, SVC, DecisionTree, ExtraTree, RandomForest, Bagging, GradientBoost and MLP.

Table 1

Classification accuracy of the learning methods combined with the FAGC module on CIFAR-10 and CIFAR-100. "Supervised" denotes that only labeled data is used to train ViT-S and ViT-T, respectively. "AVG" describes the average accuracy.

Methods	CIFAR-100				CIFAR-10			
	400 labels		2000 labels		40 labels		200 labels	
	-	+FAGC	-	+FAGC	-	+FAGC	-	+FAGC
Supervised	72.65±0.05	75.36±0.37	81.20±0.07	83.43±0.32	79.32±0.05	82.83±0.31	90.13±0.03	91.77±0.28
CoMatch[46]	62.37±0.12	68.10±0.21	80.71±0.13	82.84±0.24	88.24±0.05	90.95±0.17	93.64±0.11	94.39±0.21
Π-Model[47]	54.04±0.23	69.29±0.34	82.90±0.16	84.12±0.19	80.66±0.13	82.56±0.22	92.90±0.14	92.77±0.37
Mean Teacher[48]	70.50±0.22	75.96±0.14	81.95±0.11	83.68±0.26	81.21±0.17	84.33±0.19	92.64±0.03	92.43±0.25
Pseudo Labeling[49]	73.51±0.25	76.29±0.22	82.61±0.15	84.42±0.21	81.92±0.21	82.44±0.26	94.15±0.12	94.57±0.23
MixMatch[50]	73.87±0.32	76.06±0.15	84.07±0.21	84.58±0.34	81.81±0.25	85.07±0.19	93.83±0.16	94.31±0.31
VAT[51]	77.33±0.17	80.40±0.32	83.91±0.07	85.43±0.31	89.92±0.04	90.21±0.11	95.28±0.05	95.14±0.36
Dash[52]	78.74±0.23	82.69±0.23	86.46±0.03	87.17±0.16	93.20±0.05	93.55±0.21	95.30±0.07	95.90±0.25
CRMatch[53]	79.84±0.15	80.54±0.26	86.12±0.17	87.16±0.22	92.79±0.08	93.31±0.32	95.41±0.13	95.89±0.29
UDA[54]	80.51±0.14	82.52±0.31	86.31±0.15	87.50±0.18	91.74±0.11	92.13±0.25	95.33±0.12	95.78±0.22
FixMatch[55]	80.59±0.25	82.96±0.23	86.76±0.04	87.46±0.36	91.40±0.12	91.84±0.23	95.08±0.09	95.35±0.35
FlexMatch[56]	80.78±0.15	82.86±0.25	86.12±0.15	87.16±0.19	92.57±0.21	93.08±0.15	95.75±0.05	95.63±0.27
AdaMatch[58]	81.93±0.17	83.78±0.22	85.84±0.23	87.13±0.32	90.95±0.12	92.96±0.23	95.12±0.03	95.58±0.32
FreeMatch[57]	82.22±0.13	83.34±0.25	86.27±0.23	87.56±0.28	93.57±0.15	94.07±0.24	95.73±0.04	96.11±0.12
SimMatch[59]	82.48±0.12	83.57±0.34	86.98±0.06	87.88±0.37	92.78±0.18	93.18±0.16	95.49±0.11	95.77±0.24
SoftMatch[60]	82.72±0.11	83.11±0.28	86.83±0.17	87.81±0.26	93.27±0.11	93.68±0.12	95.72±0.16	95.55±0.34
AVG	75.88±0.17	79.18±0.25	84.69±0.13	85.96±0.26	88.45±0.13	89.76±0.21	94.46±0.09	94.81±0.27

Table 2

Comparison of classification accuracy whether to use or not use the FAGC module.

Methods	CIFAR-10						CIFAR-100					
	40 labels		200 labels		1000 labels		400 labels		2000 labels		10000 labels	
	-	+FAGC	-	+FAGC	-	+FAGC	-	+FAGC	-	+FAGC	-	+FAGC
ViT-T	79.32	82.83	90.13	91.77	96.21	96.35	63.02	66.69	74.39	76.54	80.96	82.61
ViT-S	90.00	93.31	96.45	97.12	98.19	98.26	72.65	75.36	81.20	83.43	86.28	87.39
WRN-28-2	92.89	93.77	93.92	94.17	94.30	94.58	68.92	72.09	74.73	76.33	75.59	76.21
WRN-28-8	93.29	94.51	93.32	94.53	95.32	95.68	75.73	77.21	78.82	79.56	81.23	82.12

The feature extraction network model is ViT-S, and the numbers of generated features are 10, 100, 400, 1000 and 2000. The results of these experiments are presented in Figure 4. The generated feature quantity does not exhibit a strict correlation with the model's classification accuracy. Excessive generated features can cause the model to overly focus on their distribution, but ignore the distribution of real features. Moreover, optimal performance in classification accuracy is achieved by MLP. Supplementary experiments are conducted utilizing different feature extraction models, including ViT-T and WRN-28-2. The detailed experimental results are shown in Figure 5. The results indicate that varying quantities of generated features are required by different methods, and for MLP the optimal number of generated features is 100.

4.5. Ablation study

To evaluate the influence of the generated features from the Geodesic curves on the performance of models, experiments are conducted for the 40 labeled images on the CIFAR-10. ViT-T and ViT-S are selected as feature extraction models, and MLP is employed as the final classifier. Ablation experiments are conducted on the parameter λ in the classification loss, as the Formula (10). It is noteworthy that if $\lambda = 0$, the generated features are excluded from the classification training; on the other hand, if $\lambda = 1$, the generated features are trained as real features. The experimental results are shown in Table 5. As the influence factor λ increases, the classification accuracy of the model initially rises and then exhibits a slight decline. The declining trend is attributed to the increasing influence of the generated features on the loss function, causing the model to ignore the real features.

Table 3

Comparison of the data augmentations whether to combine or not combine the FAGC module.

ID	Data augmentations						Methods	
	horizontal flip	rotate	random crop	color jitter	cutout	augmix	-	+FAGC
1	✓	✓					70.23	72.34
2			✓				70.21	73.39
3				✓			71.12	72.13
4					✓		72.14	74.93
5	✓		✓				72.65	75.36
6		✓			✓		70.11	72.28
7	✓		✓			✓	72.48	73.54
8	✓	✓	✓	✓	✓	✓	66.38	68.27

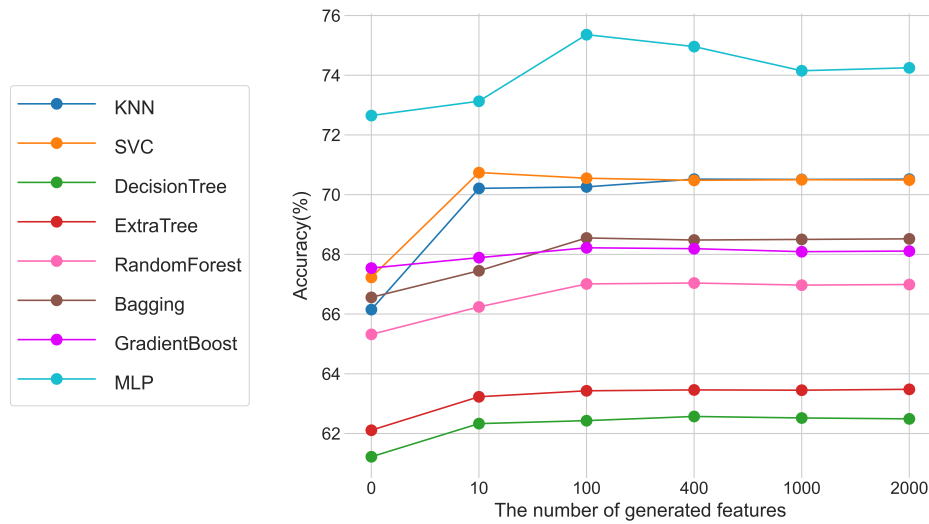


Figure 4: The classification accuracy of the different numbers of the generated features.

Table 4

Comparison of different feature classifiers on CIFAR-10.

Classifiers	CIFAR-10			
	40 labels		200 labels	
	-	+FAGC	-	+FAGC
KNN[65]	79.54	91.11	96.29	96.75
SVC[66]	89.02	91.29	96.72	96.85
DecisionTree[67]	56.76	58.51	85.62	86.03
ExtraTree[68]	51.37	66.07	78.68	85.89
RandomForest[69]	91.36	91.23	96.09	96.37
Bagging[70]	74.52	77.87	94.38	94.52
GradientBoost[71]	71.32	76.41	88.48	89.81
MLP[72]	90.00	93.31	96.45	97.12

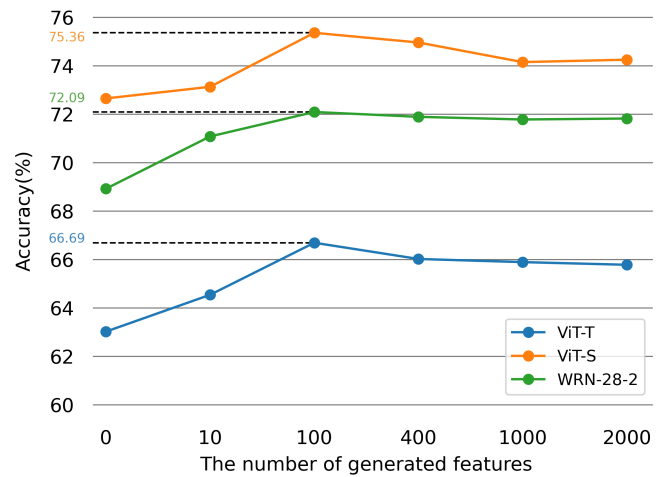


Figure 5: The classification accuracy of the different numbers of the generated features for MLP.

5. Conclusion

In this paper, we propose a data augmentation method FAGC, which can provide additional information for the models of machine learning. Experimental results show that FAGC exhibits excellent performance on different datasets.

In addition, the combination of the FAGC method with other data augmentation techniques can also achieve positive

Table 5The influence factor λ on the classification performance on CIFAR-10.

Network	λ								
	0	0.1	0.3	0.45	0.5	0.55	0.7	0.9	1
ViT-T	79.32	80.95	81.86	82.92	82.83	82.85	82.63	82.46	82.32
ViT-S	90.00	92.34	93.56	93.68	93.77	93.79	93.54	93.23	93.11

results. The enhanced generality and effectiveness can provide more comprehensive enhancement effect for machine learning tasks.

There are still potential improvements for the proposed method. For instance, the influence caused by isolated points. Alternatively, if image features are excessively scattered, and the Geodesic curve fails to reflect their distribution. It is more advisable to fit these points with a Geodesic surface. Improvements in these aspects will further boost the performance of FAGC and make it more applicable to various machine learning tasks.

References

- [1] Yann LeCun, Yoshua Bengio, and Geoffrey Hinton. Deep learning. *nature*, 521(7553):436–444, 2015.
- [2] Daniel W Otter, Julian R Medina, and Jugal K Kalita. A survey of the usages of deep learning for natural language processing. *IEEE transactions on neural networks and learning systems*, 32(2):604–624, 2020.
- [3] Mishaim Malik, Muhammad Kamran Malik, Khawar Mehmood, and Imran Makhdoom. Automatic speech recognition: a survey. *Multi-media Tools and Applications*, 80:9411–9457, 2021.
- [4] Connor Shorten and Taghi M Khoshgoftaar. A survey on image data augmentation for deep learning. *Journal of big data*, 6(1):1–48, 2019.
- [5] Olivier Rukundo and Hanqiang Cao. Nearest neighbor value interpolation. *arXiv preprint arXiv:1211.1768*, 2012.
- [6] Hongyi Zhang, Moustapha Cisse, Yann N Dauphin, and David Lopez-Paz. mixup: Beyond empirical risk minimization. *arXiv preprint arXiv:1710.09412*, 2017.
- [7] Terrance DeVries and Graham W Taylor. Improved regularization of convolutional neural networks with cutout. *arXiv preprint arXiv:1708.04552*, 2017.
- [8] Ekin D Cubuk, Barret Zoph, Jonathon Shlens, and Quoc V Le. Randaugment: Practical automated data augmentation with a reduced search space. In *Proceedings of the IEEE/CVF conference on computer vision and pattern recognition workshops*, pages 702–703, 2020.
- [9] Ian Goodfellow, Jean Pouget-Abadie, Mehdi Mirza, Bing Xu, David Warde-Farley, Sherjil Ozair, Aaron Courville, and Yoshua Bengio. Generative adversarial nets. *Advances in neural information processing systems*, 27, 2014.
- [10] Diederik P Kingma and Max Welling. Auto-encoding variational bayes. *arXiv preprint arXiv:1312.6114*, 2013.
- [11] V Terrance and W Taylor Graham. Dataset augmentation in feature space. In *Proceedings of the international conference on machine learning (ICML), workshop track*, volume 3, 2017.
- [12] Nitesh V Chawla, Kevin W Bowyer, Lawrence O Hall, and W Philip Kegelmeyer. Smote: synthetic minority over-sampling technique. *Journal of artificial intelligence research*, 16:321–357, 2002.
- [13] Chumphol Bunkhumpornpat, Krung Sinapiromsaran, and Chidchanok Lursinsap. Dbsmote: density-based synthetic minority over-sampling technique. *Applied Intelligence*, 36:664–684, 2012.
- [14] Vikas Verma, Alex Lamb, Christopher Beckham, Amir Najafi, Ioannis Mitliagkas, David Lopez-Paz, and Yoshua Bengio. Manifold mixup: Better representations by interpolating hidden states. In *International conference on machine learning*, pages 6438–6447. PMLR, 2019.
- [15] Yulin Wang, Xuran Pan, Shiji Song, Hong Zhang, Gao Huang, and Cheng Wu. Implicit semantic data augmentation for deep networks. *Advances in Neural Information Processing Systems*, 32, 2019.
- [16] David G Kendall. Shape manifolds, procrustean metrics, and complex projective spaces. *Bulletin of the London mathematical society*, 16(2):81–121, 1984.
- [17] David George Kendall, Dennis Barden, Thomas K Carne, and Huiling Le. *Shape and shape theory*. John Wiley & Sons, 2009.
- [18] DG Kendall. The diffusion of shape. 9 (3): 428-430. DOI: <https://doi.org/10.2307/1426091>, 1977.
- [19] Jun Zhang, X Zhang, Hamid Krim, and Gilbert G Walter. Object representation and recognition in shape spaces. *Pattern recognition*, 36(5):1143–1154, 2003.
- [20] Jared Glover, Daniela Rus, Nicholas Roy, and Geoff Gordon. Robust models of object geometry. *From Sensors to Human Spatial Concepts*, page 59, 2006.
- [21] Alfred Kume, Ian L Dryden, and Huiling Le. Shape-space smoothing splines for planar landmark data. *Biometrika*, 94(3):513–528, 2007.
- [22] Martin Kilian, Niloy J Mitra, and Helmut Pottmann. Geometric modeling in shape space. In *ACM SIGGRAPH 2007 papers*, pages 64–es. 2007.
- [23] Sanjeev Muralikrishnan, Siddhartha Chaudhuri, Noam Aigerman, Vladimir G Kim, Matthew Fisher, and Niloy J Mitra. Glass: Geometric latent augmentation for shape spaces. In *Proceedings of the IEEE/CVF Conference on Computer Vision and Pattern Recognition*, pages 18552–18561, 2022.
- [24] Yuexing Han, Hideki Koike, and Masanori Idesawa. Recognizing objects with multiple configurations. *Pattern Analysis and Applications*, 17:195–209, 2014.
- [25] Krishna Kumar Singh, Hao Yu, Aron Sarmasi, Gautam Pradeep, and Yong Jae Lee. Hide-and-peek: A data augmentation technique for weakly-supervised localization and beyond. *arXiv preprint arXiv:1811.02545*, 2018.
- [26] Zhun Zhong, Liang Zheng, Guoliang Kang, Shaozi Li, and Yi Yang. Random erasing data augmentation. In *Proceedings of the AAAI conference on artificial intelligence*, volume 34, pages 13001–13008, 2020.
- [27] Sangdoon Yun, Dongyoon Han, Seong Joon Oh, Sanghyuk Chun, Junsuk Choe, and Youngjoon Yoo. Cutmix: Regularization strategy to train strong classifiers with localizable features. In *Proceedings of the IEEE/CVF international conference on computer vision*, pages 6023–6032, 2019.
- [28] David G Lowe. Distinctive image features from scale-invariant keypoints. *International journal of computer vision*, 60:91–110, 2004.
- [29] Navneet Dalal and Bill Triggs. Histograms of oriented gradients for human detection. In *2005 IEEE computer society conference on computer vision and pattern recognition (CVPR'05)*, volume 1, pages 886–893. Ieee, 2005.
- [30] Gustaf Kylberg, Mats Uppström, and Ida-Maria Sintorn. Virus texture analysis using local binary patterns and radial density profiles. In *Progress in Pattern Recognition, Image Analysis, Computer Vision, and Applications: 16th Iberoamerican Congress, CIARP 2011*,

- Pucón, Chile, November 15-18, 2011. *Proceedings 16*, pages 573–580. Springer, 2011.
- [31] Pan Li, Da Li, Wei Li, Shaogang Gong, Yanwei Fu, and Timothy M Hospedales. A simple feature augmentation for domain generalization. In *Proceedings of the IEEE/CVF International Conference on Computer Vision*, pages 8886–8895, 2021.
- [32] Boyi Li, Felix Wu, Ser-Nam Lim, Serge Belongie, and Kilian Q Weinberger. On feature normalization and data augmentation. In *Proceedings of the IEEE/CVF conference on computer vision and pattern recognition*, pages 12383–12392, 2021.
- [33] Savita Ahlawat and Amit Choudhary. Hybrid cnn-svm classifier for handwritten digit recognition. *Procedia Computer Science*, 167:2554–2560, 2020.
- [34] Christopher G Small. *The statistical theory of shape*. Springer Science & Business Media, 2012.
- [35] IL Dryden and KV Mardia. *Statistical shape analysis.*(wiley: New york, ny.). 1998.
- [36] Yuexing Han, Bing Wang, Masanori Idesawa, and Hiroyuki Shimai. Recognition of multiple configurations of objects with limited data. *Pattern Recognition*, 43(4):1467–1475, 2010.
- [37] DG Kendall, H Le, D Barden, and TK Carne. *Shape and shape theory*. 1999.
- [38] Christopher G Small. *The statistical theory of shape*. *Springer Series in Statistics*, 1996.
- [39] Christopher G Small and Christopher G Small. Distributions of random shapes. *The Statistical Theory of Shape*, pages 149–172, 1996.
- [40] Jun Zhang, X Zhang, and Hamid Krim. Invariant object recognition by shape space analysis. In *Proceedings 1998 International Conference on Image Processing. ICIP98 (Cat. No. 98CB36269)*, pages 581–585. IEEE, 1998.
- [41] Yuexing Han. Recognize objects with three kinds of information in landmarks. *Pattern Recognition*, 46(11):2860–2873, 2013.
- [42] Kim Evans. *Curve-fitting in shape space. Quantitative biology, shape analysis, and wavelets*. Leeds University Press, Leeds, 2005.
- [43] Kim Kenobi, Ian L Dryden, and Huiling Le. Shape curves and geodesic modelling. *Biometrika*, 97(3):567–584, 2010.
- [44] Alexey Dosovitskiy, Lucas Beyer, Alexander Kolesnikov, Dirk Weissenborn, Xiaohua Zhai, Thomas Unterthiner, Mostafa Dehghani, Matthias Minderer, Georg Heigold, Sylvain Gelly, et al. An image is worth 16x16 words: Transformers for image recognition at scale. *arXiv preprint arXiv:2010.11929*, 2020.
- [45] Alex Krizhevsky, Geoffrey Hinton, et al. Learning multiple layers of features from tiny images. 2009.
- [46] Junnan Li, Caïming Xiong, and Steven CH Hoi. Comatch: Semi-supervised learning with contrastive graph regularization. In *Proceedings of the IEEE/CVF International Conference on Computer Vision*, pages 9475–9484, 2021.
- [47] Antti Rasmus, Mathias Berglund, Mikko Honkala, Harri Valpola, and Tapani Raiko. Semi-supervised learning with ladder networks. *Advances in neural information processing systems*, 28, 2015.
- [48] Antti Tarvainen and Harri Valpola. Mean teachers are better role models: Weight-averaged consistency targets improve semi-supervised deep learning results. *Advances in neural information processing systems*, 30, 2017.
- [49] Dong-Hyun Lee et al. Pseudo-label: The simple and efficient semi-supervised learning method for deep neural networks. In *Workshop on challenges in representation learning, ICML*, volume 3, page 896. Atlanta, 2013.
- [50] David Berthelot, Nicholas Carlini, Ian Goodfellow, Nicolas Papernot, Avital Oliver, and Colin A Raffel. Mixmatch: A holistic approach to semi-supervised learning. *Advances in neural information processing systems*, 32, 2019.
- [51] Takeru Miyato, Shin-ichi Maeda, Masanori Koyama, and Shin Ishii. Virtual adversarial training: a regularization method for supervised and semi-supervised learning. *IEEE transactions on pattern analysis and machine intelligence*, 41(8):1979–1993, 2018.
- [52] Yi Xu, Lei Shang, Jinxing Ye, Qi Qian, Yu-Feng Li, Baigui Sun, Hao Li, and Rong Jin. Dash: Semi-supervised learning with dynamic thresholding. In *International Conference on Machine Learning*, pages 11525–11536. PMLR, 2021.
- [53] Yue Fan, Anna Kukleva, Dengxin Dai, and Bernt Schiele. Revisiting consistency regularization for semi-supervised learning. *International Journal of Computer Vision*, 131(3):626–643, 2023.
- [54] Qizhe Xie, Zihang Dai, Eduard Hovy, Thang Luong, and Quoc Le. Unsupervised data augmentation for consistency training. *Advances in neural information processing systems*, 33:6256–6268, 2020.
- [55] Kihyuk Sohn, David Berthelot, Nicholas Carlini, Zizhao Zhang, Han Zhang, Colin A Raffel, Ekin Dogus Cubuk, Alexey Kurakin, and Chun-Liang Li. Fixmatch: Simplifying semi-supervised learning with consistency and confidence. *Advances in neural information processing systems*, 33:596–608, 2020.
- [56] Bowen Zhang, Yidong Wang, Wenxin Hou, Hao Wu, Jindong Wang, Manabu Okumura, and Takahiro Shinozaki. Flexmatch: Boosting semi-supervised learning with curriculum pseudo labeling. *Advances in Neural Information Processing Systems*, 34:18408–18419, 2021.
- [57] Yidong Wang, Hao Chen, Qiang Heng, Wenxin Hou, Yue Fan, Zhen Wu, Jindong Wang, Marios Savvides, Takahiro Shinozaki, Bhiksha Raj, et al. Freematch: Self-adaptive thresholding for semi-supervised learning. *arXiv preprint arXiv:2205.07246*, 2022.
- [58] David Berthelot, Rebecca Roelofs, Kihyuk Sohn, Nicholas Carlini, and Alex Kurakin. Adamatch: A unified approach to semi-supervised learning and domain adaptation. *arXiv preprint arXiv:2106.04732*, 2021.
- [59] Mingkai Zheng, Shan You, Lang Huang, Fei Wang, Chen Qian, and Chang Xu. Simmatch: Semi-supervised learning with similarity matching. In *Proceedings of the IEEE/CVF Conference on Computer Vision and Pattern Recognition*, pages 14471–14481, 2022.
- [60] Hao Chen, Ran Tao, Yue Fan, Yidong Wang, Jindong Wang, Bernt Schiele, Xing Xie, Bhiksha Raj, and Marios Savvides. Softmatch: Addressing the quantity-quality trade-off in semi-supervised learning. *arXiv preprint arXiv:2301.10921*, 2023.
- [61] Ilya Loshchilov and Frank Hutter. Decoupled weight decay regularization. *arXiv preprint arXiv:1711.05101*, 2017.
- [62] Yidong Wang, Hao Chen, Yue Fan, Wang Sun, Ran Tao, Wenxin Hou, Renjie Wang, Linyi Yang, Zhi Zhou, Lan-Zhe Guo, et al. Usb: A unified semi-supervised learning benchmark. *arXiv preprint arXiv:2208.07204*, 2022.
- [63] Sergey Zagoruyko and Nikos Komodakis. Wide residual networks. *arXiv preprint arXiv:1605.07146*, 2016.
- [64] Dan Hendrycks, Norman Mu, Ekin D Cubuk, Barret Zoph, Justin Gilmer, and Balaji Lakshminarayanan. Augmix: A simple data processing method to improve robustness and uncertainty. *arXiv preprint arXiv:1912.02781*, 2019.
- [65] Thomas Cover and Peter Hart. Nearest neighbor pattern classification. *IEEE transactions on information theory*, 13(1):21–27, 1967.
- [66] Corinna Cortes and Vladimir Vapnik. Support-vector networks. *Machine learning*, 20:273–297, 1995.
- [67] J. Ross Quinlan. Induction of decision trees. *Machine learning*, 1:81–106, 1986.
- [68] Pierre Geurts, Damien Ernst, and Louis Wehenkel. Extremely randomized trees. *Machine learning*, 63:3–42, 2006.
- [69] Leo Breiman. Random forests. *Machine learning*, 45:5–32, 2001.
- [70] Leo Breiman. Bagging predictors. *Machine learning*, 24:123–140, 1996.
- [71] Jerome H Friedman. Greedy function approximation: a gradient boosting machine. *Annals of statistics*, pages 1189–1232, 2001.
- [72] David E Rumelhart, Geoffrey E Hinton, and Ronald J Williams. Learning representations by back-propagating errors. *nature*, 323(6088):533–536, 1986.